Robust Identification of Local Biogeophysical Effects of Land-Cover Change in a Global Climate Model

J. WINCKLER, C. H. REICK, AND J. PONGRATZ

Max Planck Institute for Meteorology, Hamburg, Germany

(Manuscript received 14 January 2016, in final form 21 September 2016)

ABSTRACT

Land-cover change (LCC) happens locally. However, in almost all simulation studies assessing biogeophysical climate effects of LCC, local effects (due to alterations in a model grid box) are mingled with nonlocal effects (due to changes in wide-ranging climate circulation). This study presents a method to robustly identify local effects by changing land surface properties in selected ''LCC boxes'' (where local plus nonlocal effects are present), while leaving others unchanged (where only nonlocal effects are present). While this study focuses on the climate effects of LCC, the method presented here is applicable to any land surface process that is acting locally but is capable of influencing wide-ranging climate when applied on a larger scale. Concerning LCC, the method is more widely applicable than methods used in earlier studies. The study illustrates the possibility of validating simulated local effects by comparison to observations on a global scale and contrasts the underlying mechanisms of local and nonlocal effects. In the MPI-ESM, the change in background climate induced by extensive deforestation is not strong enough to influence the local effects substantially, at least as long as sea surface temperatures are not affected. Accordingly, the local effects within a grid box are largely independent of the number of LCC boxes in the isolation approach.

1. Introduction

Humans have altered the land surface extensively by changing land cover, for example, by replacing forests with grasslands (e.g., Pongratz et al. 2008). Such land-cover change (LCC) not only affects the carbon balance (IPCC 2013) but also disturbs the energy and hydrological balance of the land surface via biogeophysical (BGP) effects: First, surface albedo increases when replacing a forest with typically brighter grassland, reflecting more sunlight and altering the surface shortwave radiation budget (e.g., Bonan 2008). Second, LCC induces changes in nonradiative properties, such as evapotranspiration efficiency [as defined in the study by Davin and de Noblet-Ducoudré (2010)] and surface roughness. These biogeophysical effects can alter climate within a grid box undergoing LCC, which we refer to as the local effects. However, in addition to these locally induced effects, climate within a grid box can also be altered by LCC in nearby or remote grid boxes, which we refer to as nonlocal effects.

In the past, two types of studies have been performed to quantify and understand the effects of LCC: studies investigating plausible LCC scenarios and studies investigating idealized extensive LCC. The first type investigated the climate effects of plausible LCC scenarios such as the historical evolution of land-use-induced LCC or future LCC (e.g., Pitman et al. 2009; Boysen et al. 2014), based on scenarios derived from socioeconomic models (e.g., Hurtt et al. 2011). Considering temperature on the local scale, the BGP effects of historical LCC have been simulated to have similar magnitude as the effect of the increase in greenhouse gases since the preindustrial period (de Noblet-Ducoudré et al. 2012). However, models do not agree in sign and amplitude of temperature changes following land-use-induced LCC, neither regionally nor globally (e.g., Pitman et al. 2009; Boysen et al. 2014). Part of the uncertainty in studies on plausible LCC scenarios originates from the fact that in most grid boxes, these scenarios alter only a small fraction of the vegetation cover. This results in a climatic signal that is small compared to weather-related noise, especially as regions with a large historical land-use-induced LCC are located in the northern temperate latitudes, where weather-related noise is high (e.g., Mahlstein et al. 2011).

Corresponding author e-mail: J. Winckler, johannes.winckler@mpimet.mpg.de

DOI: 10.1175/JCLI-D-16-0067.1

The second type of LCC study investigated the effects of idealized extensive (instead of plausible) LCC, such as complete deforestation of wide latitudinal bands (e.g., Claussen et al. 2001; Bala et al. 2007; Bathiany et al. 2010), with a focus on understanding the more general role of vegetation changes in the Earth system. While such idealized simulations improve the signal-to-noise ratio, they also feature substantial nonlocal effects because extensive changes in surface properties can alter global circulation (e.g., Goessling and Reick 2011; Swann et al. 2012). Within a region, the nonlocal effects can even be larger than the local effects of deforestation (Devaraju et al. 2015). However, in the traditional approach of simulating spatially homogeneous LCC in every grid box within a large region, local and nonlocal effects are mingled and cannot be distinguished. This brings complications: Observations of LCC effects comprise only the local LCC effects because they compare climate in forested areas with nearby open land, and thus both weather-related noise and nonlocal effects cancel. Thus, the total (local plus nonlocal) simulated effects cannot be compared to observations consistently. In addition, simulations of idealized extensive LCC cannot represent the effects of any plausible LCC scenario owing to substantial nonlocal effects. In particular, with the model setup used in most previous studies, the results within a grid box are not only determined by the extent of LCC within that grid box but also strongly dependent on LCC in neighboring or remote grid boxes (see, e.g., the boreal cooling simulated for tropical deforestation due to a reduction in atmospheric water vapor; Claussen et al. 2001). Therefore, the total effect of LCC within a grid box strongly depends on the chosen geographical distribution of LCC boxes, impeding inference of the climatic relevance of LCC in a specific grid box from one global LCC distribution to the other.

The local effects have been implicitly isolated for historical and future projected LCC (Kumar et al. 2013) in order to deal with the problem of low signal-to-noise ratio in plausible LCC scenarios. Similar to observational studies, Kumar et al. 2013 compare climatic changes in grid boxes with LCC to climatic changes in grid boxes without LCC within a region where changes in climatic conditions are assumed to be homogeneous, and thus both weather-related noise and nonlocal effects cancel. Malyshev et al. (2015) isolate local effects in a model that calculates canopy air temperature separately for each land-use type within a grid box. They calculate local effects as the temperature difference between the different land-use types within a grid box. Furthermore, they compare their local effects with the total effects that result from the typical model setup of earlier studies comparing a simulation with LCC to a reference with undisturbed vegetation. Here, we present a method to isolate the local effects by specifying regularly spaced ''LCC boxes'' (where both local plus nonlocal effects are present) and ''no-LCC boxes'' (where only nonlocal effects are present). The presented approach goes beyond the previous approaches in several respects: First, it provides information on the local effects in every land grid box globally and avoids applying ad hoc thresholds in the amount of LCC to identify areas of LCC as in the study by Kumar et al. (2013). Second, our setup captures all simulated land–atmosphere feedbacks within a grid box, even via local changes in clouds and precipitation. This complements previous studies calculating local effects using offline models (e.g., West et al. 2011) or a subgrid tile approach as in the study by Malyshev et al. (2015). Third, our method is applicable to all DGVMs, even if they do not calculate temperature for each subgrid tile separately, as in the study by Malyshev et al. (2015).

In this study, we examine the sensitivity of the local effects to the number of LCC boxes used in this separation method. Potentially, a high number of LCC boxes could change background climate strong enough to influence the local effects (Pitman et al. 2011). We assess whether the change in background climate via the nonlocal effects is strong enough to influence the local effects substantially or whether we can still robustly identify the local effects. To this end, we compare the local effects in two extreme cases: LCC only at a few grid boxes, similar to plausible LCC scenarios, and LCC in almost all grid boxes, representative for idealized extensive LCC. If the local effects can be identified irrespective of the number of LCC boxes, this isolation is a step toward consistent comparison of LCC effects between models and observational datasets. The presented method allows us to isolate the local effects but also to additionally quantify the nonlocal effects. This separation of local and nonlocal effects opens ways for a better understanding of the processes underlying the climatic effects of LCC and related interactions with local and large-scale climate.

2. Methods

a. *Model and setup*

We use the Max Planck Institute Earth System Model (MPI-ESM), which has been validated in depth with respect to the energy and hydrological balance at the land surface by Hagemann et al. (2013). Deforestation effects in an offline land surface model differ substantially from the results in a setup accounting for atmospheric feedbacks (Gibbard et al. 2005). Thus, we choose a configuration with the land surface model JSBACH (Reick et al. 2013) coupled to the atmospheric

model ECHAM6 (Giorgetta et al. 2013) with a spectral horizontal resolution of T63 (approximately 2° at the equator) and 47 vertical layers. In each simulation, we use the last 30 out of 35 years (1976–2005) for analysis. To exclude carbon effects of LCC and thus isolate the BGP effects, we prescribe CO_2 from the historical simulation performed within phase 5 of the Coupled Model Intercomparison Project (CMIP5) by the fully coupled MPI-ESM. From this simulation, we also prescribe 1976–2005 interannually varying SSTs and sea ice in order to reduce weather-related noise induced by ocean variability. A similar setup has been used in an intercomparison of the BGP effects of historical land-use-induced LCC, where ECHAM5/JSBACH was within the range of the other models, both for radiative and nonradiative processes (Boisier et al. 2012). Prescribing SST substantially influences simulated LCC effects (Davin and de Noblet-Ducoudré 2010). Nevertheless, SSTs are intentionally prescribed in our study in order to identify the local effects of LCC more clearly—only the nonlocal effects are affected by land–ocean interactions. This issue is further discussed in the discussions and conclusions section.

As described in the next paragraph, we choose two setups, in each of which land cover is changed in some grid boxes (LCC boxes) and remains unchanged in other grid boxes. For each of the two spatial distributions of LCC boxes described below, we perform two simulations: In the first simulation, we set the vegetated part in the LCC boxes to 100% forest cover. In the second simulation, we set the vegetated part of the LCC boxes to 100% grass cover. When scaling to 100% grass cover, we keep the ratio between C3 and C4 grasses, and when scaling to 100% forest cover, we keep the ratio between the four forest PFTs in JSBACH (tropical broadleaf evergreen, tropical broadleaf deciduous, extratropical evergreen, extratropical deciduous). In the remaining no-LCC boxes we do not change land cover but prescribe present-day land cover (the CMIP5 mean state of 1976–2005) in both simulations. We calculate the total deforestation effect as the difference between these two simulations. This simulated LCC effect, prior to the separation of local and nonlocal effects, is what we call the ''signal'' in the following.

b. Definition of sparse and extensive LCC

We are interested in the local LCC effects. The most accurate way to directly simulate these local effects at a given grid box would be to simulate LCC at only this one grid box. However, this would require one ''forest'' and one ''grass'' simulation for each land grid box. Our approach to reduce the number of required simulations is to change land cover in more than one land grid box per simulation pair. First, we deforest one out of eight grid boxes (gray grid boxes in Fig. 1b), which we define as sparse LCC. The local effects can then be separated as described in the next subsection. This scheme of sparse LCC is a trade-off: by deforesting only a small number of grid boxes, we can assume that the deforestation effects of any two boxes do not influence each other substantially, but we can still get information about the local effects on a global scale.

The choice of one out of eight LCC boxes seems arbitrary. To test the sensitivity of the local effects to the number of LCC boxes, we choose an additional scheme of deforestation in seven out of eight grid boxes (gray grid boxes in Fig. 1g), which we define as extensive LCC. This choice of the extensive LCC scheme is again a trade-off: it approximates the case of the maximal possible number of LCC boxes but still allows us to separate local and nonlocal effects, as explained below. The two LCC schemes differ only in the number of LCC boxes. We prescribe the same SSTs as in the sparse LCC case in order to ensure comparability of the results.

c. Separation of local and nonlocal effects

We define the local effects within a grid box as the changes that are present only as a result of changes in surface properties of only this one grid box. We define the nonlocal effects as LCC-induced changes that arise remotely from the location of LCC, mediated, for example, by induced changes in circulation. In our setup of introducing LCC only in the LCC boxes, nonlocal effects may be active in both LCC boxes and no-LCC boxes. In the following, we assume that the simulated total signal in LCC boxes consists of the sum of local and nonlocal effects, while the simulated signal in no-LCC boxes consists of only nonlocal effects.

Several computational steps are necessary to separate local and nonlocal contributions to the total effect of LCC. These steps are illustrated in Fig. 1:

- Figure 1a, from the described pair of simulations we identify the LCC signal.
- Figure 1b, the nonlocal effects can be seen in the no-LCC boxes (colored grid boxes in Fig. 1b).
- Figure 1c, we assume that these nonlocal effects are present also in the LCC boxes. We obtain the nonlocal effects in the LCC boxes by horizontal interpolation.
- Figure 1d, we then calculate the local effects in the LCC boxes. To this end, we assume that both local and nonlocal effects are present within the LCC boxes. Consequently, in order to obtain the local effects in the LCC boxes, we subtract the nonlocal effects, as calculated in the previous step, from the total simulated (local plus nonlocal) signal.

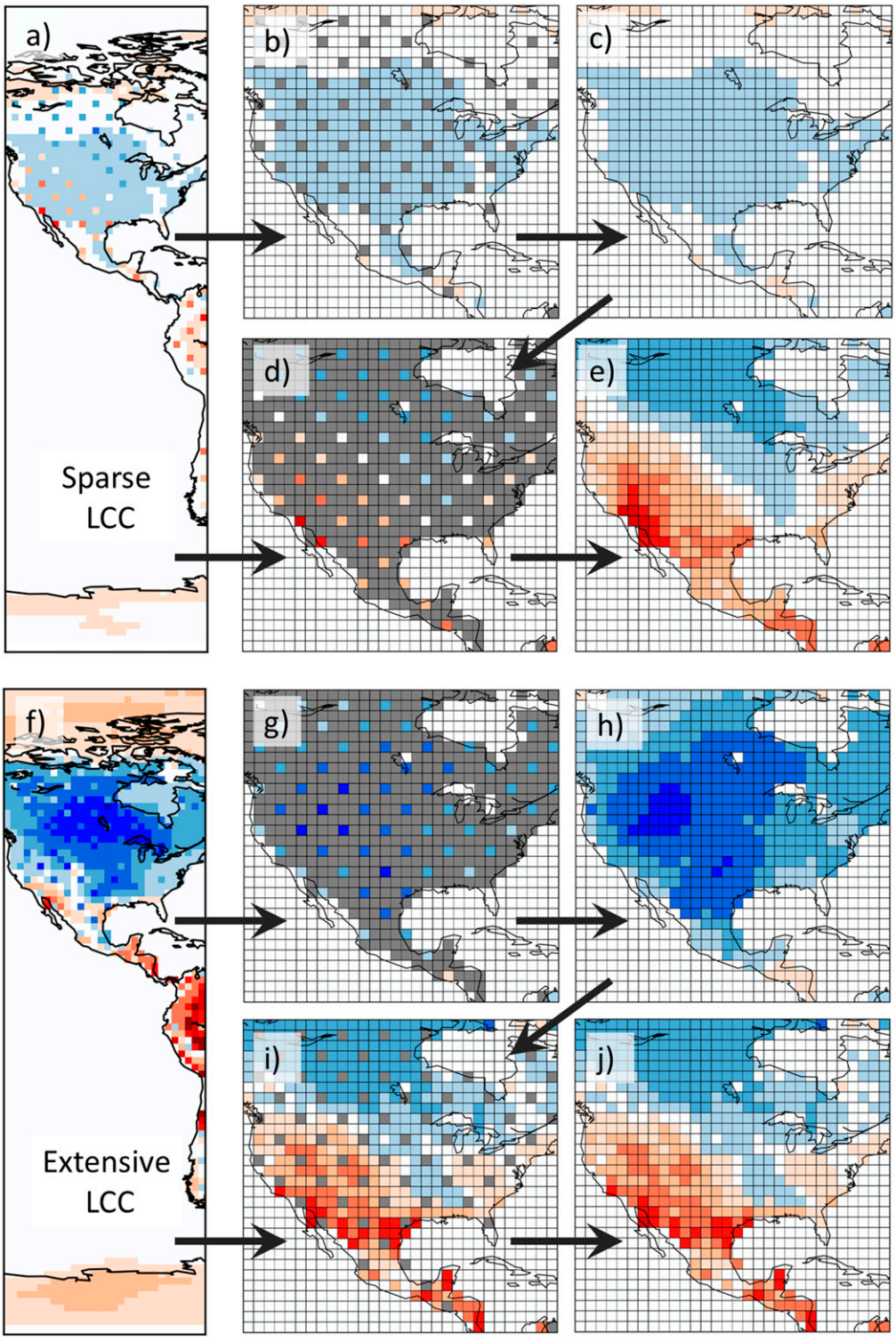

FIG. 1. Sketch illustrating the separation approach (arbitrary color scale). (a) The simulated signal. The LCC grid boxes stand out because there the signal (local plus nonlocal) is mostly stronger than in the surrounding non-LCC grid cells (only nonlocal). (b) The nonlocal effects at no-LCC boxes. (c) The nonlocal effects are interpolated to LCC boxes. (d) The difference at the LCC boxes between the simulated signal in (a) and interpolated nonlocal effects in (c) is shown, which we then (e) interpolate in order to obtain global information on the local effects. This approach works analogously for extensive deforestation [(f)–(j)]. Grid boxes whose information is not used for interpolation in (b),(d),(g),(i) are shown in gray. (For results on local and nonlocal effects see Fig. 2.)

Figure 1e, we obtain a global map of the local effects by interpolation of the identified local effects from the LCC boxes to all land grid boxes.

The local contribution to the total LCC signal is in a statistical sense ''cleaner'' than the total simulated signal; for the total simulated signal a longer simulation period is needed to decrease the signal-to-noise ratio compared to the signal-to-noise ratio of the local effects (Fig. A1) because climate variability (e.g., Deser et al. 2012) is by construction mostly contained in the nonlocal effects. Simulating time periods longer than 30 years does not increase the signal-to-noise ratio for the local effects, as demonstrated in appendix A.

Both approaches, sparse and extensive LCC, include horizontal interpolation from one out of eight grid boxes (for the interpolation of local or nonlocal effects, respectively). The error associated with interpolation depends on the distance between the interpolation knots (i.e., the distance between the grid boxes that the values are interpolated from). To assess the interpolation errors in the performed simulations, and to decrease dependence on the location of the LCC boxes, we repeat all simulations with the LCC boxes shifted by two. For further analysis, we average local effects obtained from the unshifted and shifted simulations and apply the same averaging to the nonlocal effects. Details on the interpolation method and interpolation errors are presented in appendix D.

d. *Energy balance decomposition*

In the presented results, we contrast the mechanisms underlying local and nonlocal effects. For the exploration of these mechanisms, we employ an energy balance decomposition approach as in, for example, the study by Luyssaert et al. (2014). Here, we provide a short introduction to this method, in which a change in simulated surface temperature can be split into contributions from the individual terms of the surface energy balance.

The surface energy budget is balanced between shortwave and longwave net radiation SW_{net} and LW_{net}, latent heat LE, sensible heat H, and a residual term G (mainly consisting of ground heat flux):

$$SW_{net} + LW_{net} = LE + H + G. \quad (1)$$

The component LW_{net} can be rewritten by applying the Stefan–Boltzmann law:

$$LW_{net} = \varepsilon LW_{down} - LW_{up} = \varepsilon LW_{down} - \sigma\varepsilon T_{surf}^4, \quad (2)$$

where σ is the Stefan–Boltzmann constant, ε is emissivity and is set to 1, and T_{surf} is surface temperature. Inserting (2) into (1), we obtain

$$\sigma T_{surf}^4 = SW_{net} + LW_{down} - LE - H - G.$$

Applying the total derivative and expanding with the difference ΔT_{surf}, we obtain

$$\Delta T_{surf} = \frac{1}{4\sigma T_{surf}^3}(\Delta SW_{net} + \Delta LW_{down} - \Delta LE - \Delta H - \Delta G).$$

As the multiyear mean ground heat flux is largely unaffected by deforestation (not shown), we omit the residual term ΔG in the following analysis. Note that the energy balance decomposition approach does not allow us to attribute changes in the energy balance to changes in surface properties. As an example, a simulated change in LE could originate from a change in surface albedo, evapotranspiration efficiency, surface roughness, or a combination of all three (Davin and de Noblet-Ducoudré 2010). However, the surface energy balance decomposition illustrates the importance of changes in the individual flux terms that each are influenced by changes in various surface properties and include feedbacks.

3. Contrasting local and nonlocal effects of global deforestation

a. *Mechanisms underlying local and nonlocal effects differ*

To study the effects of global deforestation, we contrast the local and nonlocal effects from the extensive LCC experiment. The local effects of deforestation on surface temperature in ECHAM6/JSBACH are a warming in the tropics and a cooling in the northern high latitudes (Fig. 2b). This is in accordance with the local effects shown in the study by Malyshev et al. (2015) and qualitatively also in accordance with previous idealized extensive LCC studies that considered the total (local plus nonlocal) effects (e.g., Claussen et al. 2001; Davin and de Noblet-Ducoudré 2010). The dynamic global vegetation model JSBACH is known to underestimate bare land fraction in subtropical deserts (Brovkin et al. 2013), which explains why there are still substantial local effects in these regions. Note that 2-m air temperature responds much more weakly to LCC as compared to surface temperature (see appendix C). Precipitation decreases in the local effects in the northern temperate and boreal regions, and even more strongly in the humid tropics (Fig. 3b). Concerning the total effects, most previous studies hinted at a decrease in rainfall (e.g., for deforestation of the Amazon rain forest; Lejeune et al. 2015).

The nonlocal effects for surface temperature (Fig. 2d) and precipitation (Fig. 3d) are similar in magnitude as

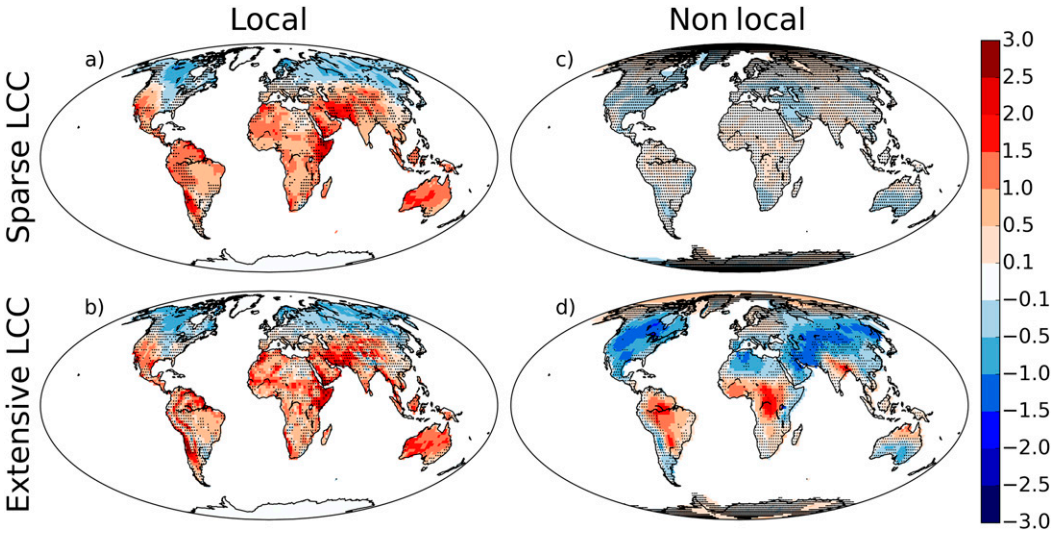

FIG. 2. Change in mean surface temperature (K) due to (a),(c) sparse and (b),(d) extensive deforestation. (a),(b) Local effects and (c),(d) nonlocal effects. Mean over 30 years and another 30 years from a simulation with LCC boxes shifted by two. Statistical significance is calculated according to a 5% level in Student's *t* test accounting for autocorrelation (Zwiers and von Storch 1995). Note that we mark grid boxes that are not statistically significant.

compared to the local effects. While for both effects temperature is increased and precipitation is reduced in the Amazon region and central Africa, there are also regions where local and nonlocal effects disagree significantly in sign (Fig. 2b vs Fig. 2d; Fig. 3b vs Fig. 3d). These are, for example, the southern part of Australia, where the local effects show a warming while the nonlocal effects are cooling, or the Malay Archipelago, where the local effects show a decrease in precipitation while the nonlocal effects show an increase in precipitation.

Not only the spatial patterns but also the mechanisms underlying local and nonlocal effects differ. Considering, for example, the local effects in the boreal winter months DJF (Fig. 4b for extensive LCC), we obtain an increase in surface temperature south of 40°N. In the arid tropics (e.g., Fig. B5d), this warming can be attributed to changes in surface sensible heat flux, probably

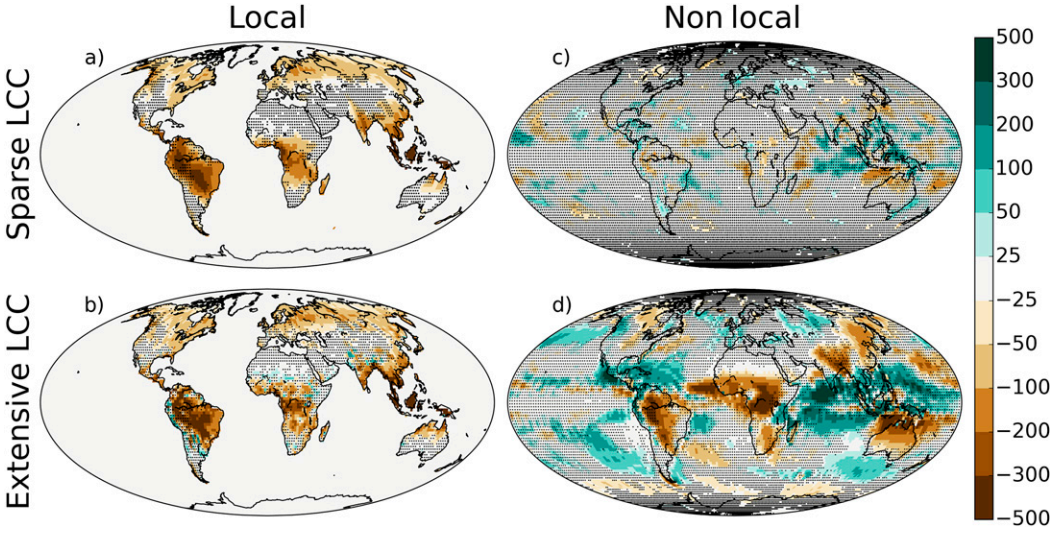

FIG. 3. Change in mean precipitation (mm yr^{-1}) for (a),(c) sparse and (b),(d) extensive deforestation. (a),(b) Local effects and (c),(d) nonlocal effects. Statistical significance is calculated according to a 5% level in Student's *t* test accounting for autocorrelation (Zwiers and von Storch 1995). Note that we mark grid boxes that are not statistically significant, and note the nonlinear scale.

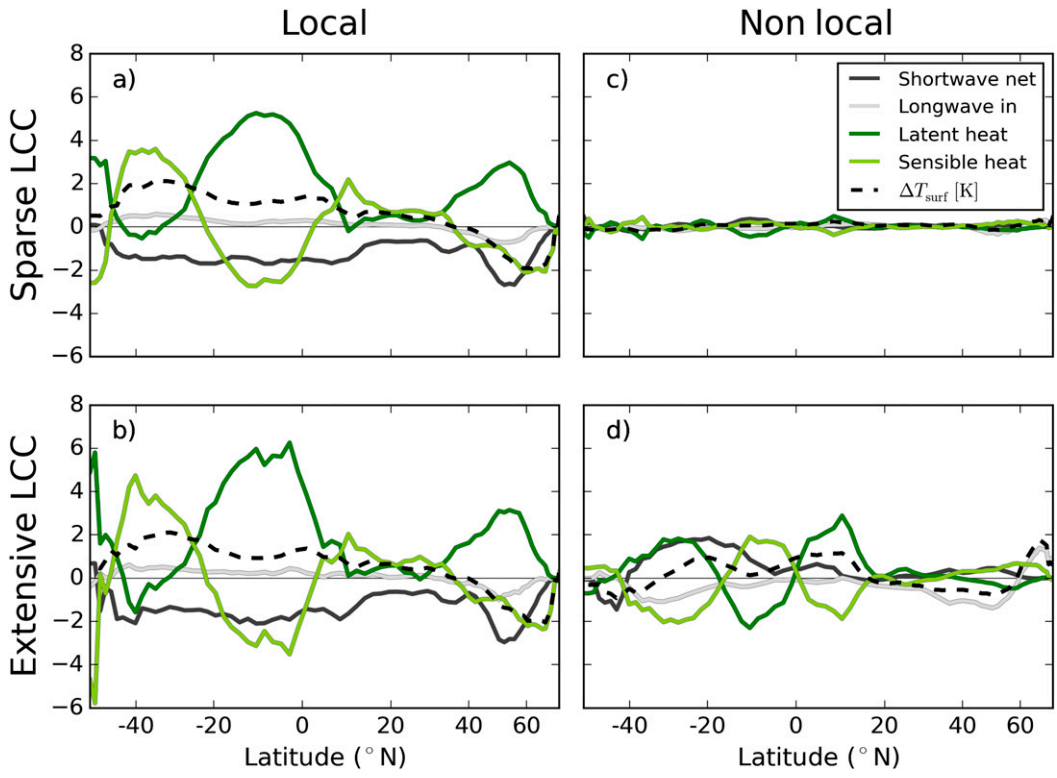

FIG. 4. Energy balance decomposition for the boreal winter months (DJF). The dashed line denotes changes in surface temperature T_{surf} (K), caused by (a),(c) sparse and (b),(d) extensive deforestation. (a),(b) Local effects, and (c),(d) nonlocal effects. The solid lines, which approximately add up to the dashed line, represent surface temperature changes due to changes in components of the surface energy budget. All values are latitudinally averaged over land areas. The horizontal axis is scaled with the area that the respective latitude occupies.

triggered by a reduction in surface–atmosphere exchange of heat because of a decreased surface roughness, consistent with the study by Rotenberg and Yakir (2010). In the humid tropics (e.g., Fig. B5c), the response is dominated by changes in latent heat flux, probably triggered by changes in evapotranspiration efficiency. North of 40°N, the surface cooling of the local effects partly originates from a strong decrease in surface shortwave net radiation due to the albedo increase after deforestation, which is especially strong in the presence of snow (not shown). Considering the nonlocal effects (Fig. 4d), we see that the underlying mechanisms differ from the local effects: The changes in latent and sensible heat in the tropics indicate a southward shift of the tropical rainbands (not shown). In contrast to the local effects, increased surface shortwave and decreased longwave net radiation hint at a reduction in atmospheric water vapor and cloud cover.

The processes underlying local and nonlocal effects are inherently different. While nonlocal effects are driven by changes in global or regional climatic conditions, local effects result from changes in local surface properties and are only enhanced or weakened by changes in local climate conditions. Both for local and nonlocal effects, the mechanisms vary between regions and seasonally (see appendix B). This analysis is not meant to be exhaustive but demonstrates that the mechanisms underlying local and nonlocal effects differ. Thus, it is important to distinguish local and nonlocal effects of LCC in Earth system simulations aimed at process understanding.

b. *Local effects enable consistent comparison with observations*

Because of the limited availability of time series covering LCC, observational studies often approximate LCC effects from a ''paired-site setup'' (i.e., from the difference in climate variables in adjacent locations with the same background climate but different land cover; e.g., Lee et al. 2011; Li et al. 2015). Thus, by construction, these observational studies cover only the local effects. The presence of nonlocal effects has impeded validation of the effects of simulated extensive deforestation with observational datasets in past studies (Zhang et al. 2014). Thus, isolation of local effects enables a more consistent comparison of deforestation

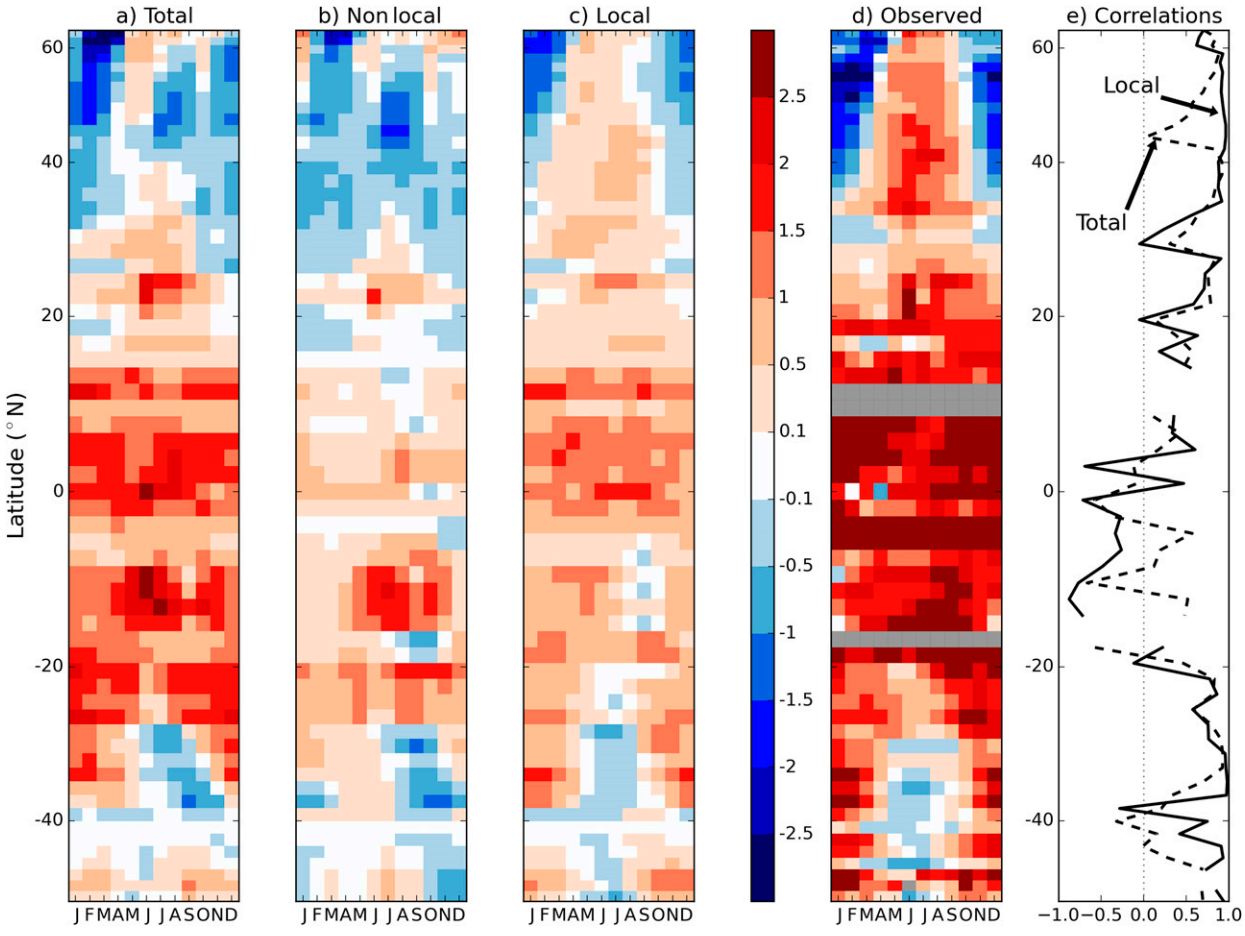

FIG. 5. Surface temperature change (K) of deforestation for (a) the total effects (local plus nonlocal effects), (b) the nonlocal effects, (c) the local effects, evaluated where observations were available, (d) remote sensing observations from Li et al. (2015, their Fig. 2c), with the latitudes regridded to our model resolution, and (e) correlation coefficient of the monthly means (averaged over the available time period) in the respective latitudes for observations vs local (solid) and observations vs total effects (dashed). The vertical axis is scaled with the area that the respective latitude occupies.

effects against observations, as noted by Malyshev et al. (2015).

In Fig. 5, we compare the local effects from the extensive LCC setup with paired-site observations from Li (2016). In Li et al.'s (2015) observational study, they investigate the local effects of deforestation on a global scale by comparing surface temperature of forest with that of open land within a small region (approximately 50 km × 28 km based on MODIS satellite imagery). In the model, the simulated local response (Fig. 5c) is weaker than in the observations (Fig. 5d) in most seasons and latitudes, part of which can be explained by the fact that the observational dataset only captures clear-sky conditions (Li et al. 2015). Nevertheless, local effects in ECHAM6/JSBACH and observations generally agree with respect to the seasonal pattern in the extratropics. However, in the tropics, seasonal cycles do not match, which becomes evident in low temporal correlations (northern tropics) or even negative temporal correlations (southern tropics) between simulated local effects and observations (Fig. 5e). Both the high correlation in the extratropics (at around 30°–45°N) and the low correlation in the tropics (at around 5°–15°S) are less evident when comparing observations to the total (local plus nonlocal) effects, and thus a more thorough assessment is enabled by isolation of the local effects. This once more puts emphasis on the importance of isolating the local effects when comparing simulated deforestation effects to observational datasets.

c. *Dependence of nonlocal and local effects on the number of LCC boxes*

The comparison of sparse and extensive LCC shows that nonlocal effects strongly depend on the areal extent of LCC. For sparse LCC, the nonlocal effects have the order of magnitude of weather-related noise in almost

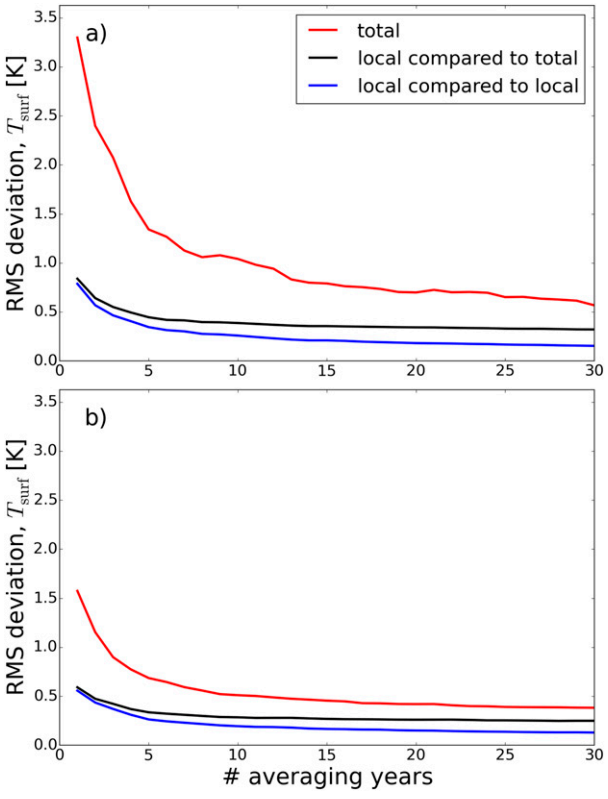

FIG. A1. Root-mean-square deviation of surface temperature T_{surf} (K) for (a) January and (b) July over all land areas. The lines show means of the combinations of the five ensemble members. The *y* axis denotes the number of averaging years.

all regions, as shown by the small number of significant grid boxes (Figs. 2c and 3c). For extensive LCC, the nonlocal effects have the same order of magnitude as the local effects. In contrast, the local effects within this setup do not differ substantially between sparse and extensive LCC (Fig. 2a vs Fig. 2b). This is the case for changes in not only surface temperature but also precipitation (Fig. 3a vs Fig. 3b) and 2-m air temperature (Fig. C1a vs Fig. C1b).

To quantify the similarity of the local effects in the two LCC cases, we determine the mean absolute difference of surface temperature over land between local effects from extensive and sparse LCC, respectively. We compute the numbers below only from values at the sparse LCC boxes in both cases in order to reduce differences due to the different number of LCC boxes. The mean absolute difference between the two local effects is 0.15 K and thus of secondary importance as compared to the effect itself (the mean absolute change in surface temperature on land for the local effects in the sparse LCC is 0.69 K). There is no systematic bias: the mean difference between local effects for sparse versus extensive LCC is 0.05 K. At the same time, spatial correlation between the two is 0.96, so also the spatial patterns of the local effects is practically identical for the two LCC cases.

Not only the spatial patterns but also the mechanisms underlying the local effects are identical for sparse and extensive LCC, as can be seen in Fig. 4a versus Fig. 4b. The peaks are more pronounced for extensive LCC (Fig. 4b) because of the different number of LCC boxes that the local effects are interpolated from. Still, the latitudinal patterns of the energy balance decompositions match well for the local effects from sparse and extensive LCC, illustrating that the underlying mechanisms are the same. Therefore, on the gridbox level, the local effects are largely independent of the number of LCC boxes in the separation approach, although background climate is strongly influenced by the nonlocal effects owing to the grossly differing areal LCC extent. While an even stronger change in background climate than can be induced by LCC might be capable of influencing the local effects, our results suggest that—at least in the case of unaffected SSTs—the local effects on a gridbox level will be robust for a wide range of chosen numbers of LCC boxes in the separation approach.

4. Discussion and conclusions

In simulations of idealized extensive LCC, local effects are masked by the strong presence of nonlocal effects. The results presented here confirm previous studies (e.g., Swann et al. 2012; Devaraju et al. 2015) that illustrate that the sum of LCC on a larger scale can trigger substantial nonlocal effects. However, the effects of deforestation of a single model grid box are initially local. Thus, the total simulated effects of large-scale LCC are not representative for the effects of deforestation in plausible LCC scenarios, in which nonlocal effects are less pronounced. Previous studies have focused on isolating the local—that is, locally induced—biogeophysical climate effects of LCC, either in plausible LCC scenarios (Kumar et al. 2013) or in models with climate information on subgrid vegetation tiles (Malyshev et al. 2015). Here, we present a method that is capable of robustly isolating the local effects, accounting for local atmospheric feedbacks. Our results, based on two extreme cases of LCC (sparse and extensive), suggest that the local effects in MPI-ESM can be robustly isolated irrespectively of the number of LCC boxes. Thus, follow-up studies that require an isolation of the local effects may use a chessboard-like pattern of one out of two LCC boxes (see appendix D) in order to only rely on interpolation from directly adjacent grid boxes and thus reduce the horizontal interpolation errors.

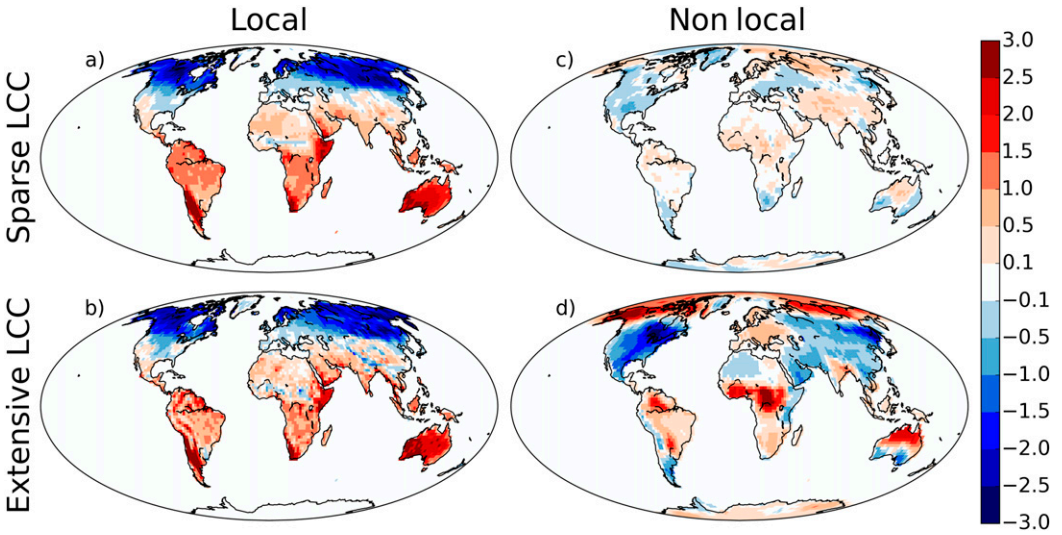

FIG. B1. Boreal winter (DJF) change in mean surface temperature (K) due to (a),(c) sparse and (b),(d) extensive deforestation. (a),(b) Local effects and (c),(d) nonlocal effects. Mean over 30 years and another 30 years from a simulation with LCC boxes shifted by two.

Interpretation of the nonlocal effects is more complex than interpretation of the local effects for several reasons: First, for the nonlocal effects of one concrete geographical distribution of LCC, we cannot determine the relative importance of LCC of each grid box for triggering those nonlocal effects. Second, while the nonlocal effects are determined by a modification of wide-ranging meteorological relationships, the local effects within a grid box can be largely explained directly by changes in local surface properties. Thus, we can understand the mechanisms underlying the local effects better than those underlying the nonlocal effects. Third, the nonlocal effects depend not only on the spatial extent but also strongly on the concrete geographical LCC distribution because LCC changes atmospheric circulation. This impedes inference of the climatic relevance of LCC from one LCC distribution to the other. We have shown that the local effects within a grid box can be robustly isolated using a wide range of spatial LCC patterns, even in the presence of substantial nonlocal effects. This is a step toward a better attribution of climatic changes to local LCC. This attribution is important, as there are various plausible scenarios for future LCC (Hurtt et al. 2011). Independent of the investigated

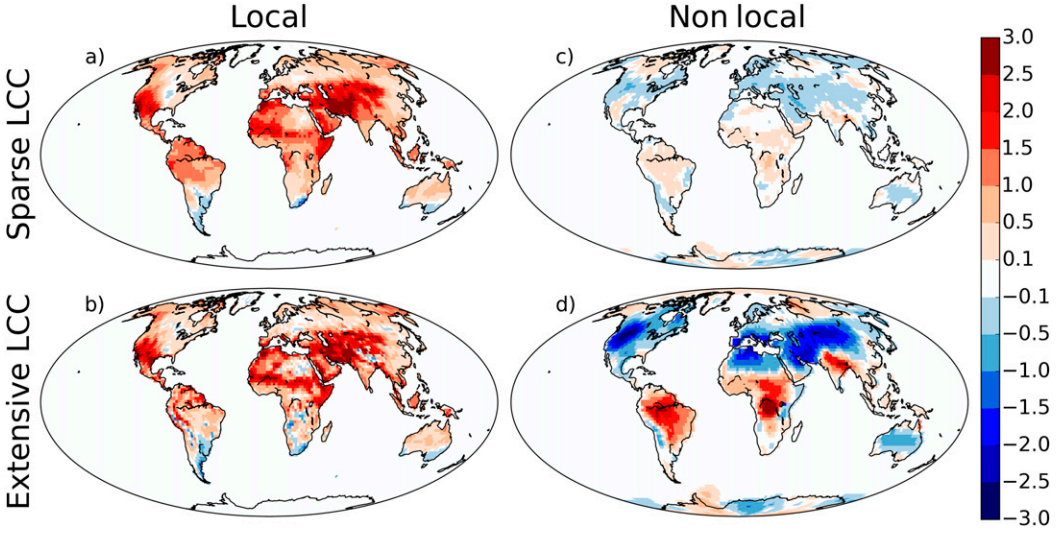

FIG. B2. As in Fig. B1, but for boreal summer (JJA).

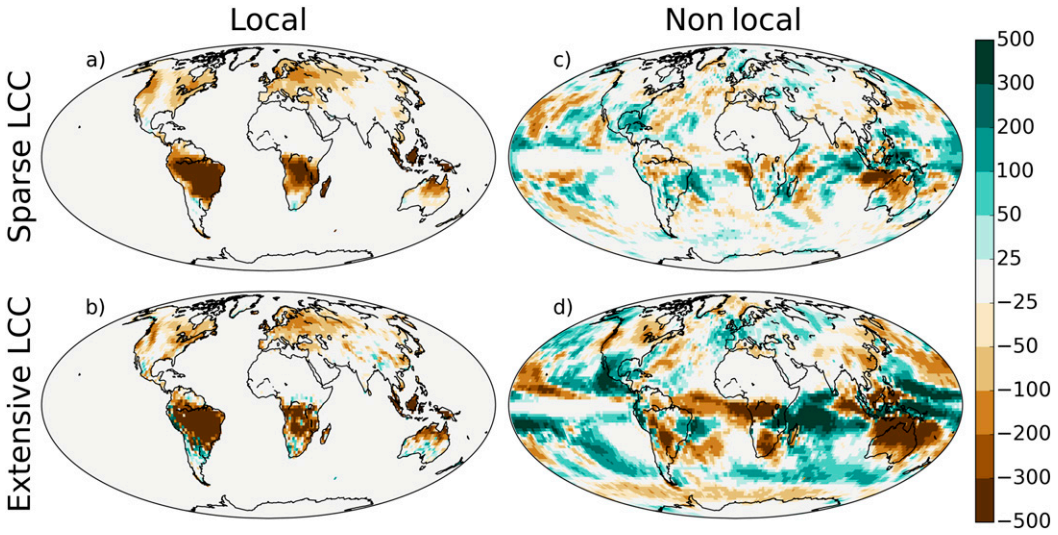

FIG. B3. As in Fig. B1, but for change in mean precipitation (mm yr^{-1}). Note the nonlinear scale.

scenario, the local effects thus allow for an assessment in an adaptation/mitigation context.

Changes in background climate can influence the effects of LCC (Pitman et al. 2011). To isolate the local effects, we want to keep LCC-induced changes in background climate small, and thus we prescribe SSTs. In this setup of prescribed SSTs, the local effects are very similar for sparse and extensive LCC, indicating that changes in background climate by extensive LCC are not strong enough to substantially influence the local effects. It is not clear if this conclusion still holds with an interactive ocean; accounting for oceanic feedbacks in a global deforestation experiment has been simulated to influence deforestation effects (1 K less tropical warming and about 2 K more Northern Hemispheric cooling in one climate model; Davin and de Noblet-Ducoudré 2010). We speculate that, if we used interactive SSTs in our simulations, most of these feedbacks would be included in the nonlocal effects, as they would also be seen in hypothetical no-LCC boxes. The oceanic feedback strength from the study by Davin and de Noblet-Ducoudré (2010) would thus lead to approximately a doubling of the nonlocal effects in terms of surface temperature changes. To avoid an influence of these amplified nonlocal effects on the local effects, we recommend prescribing SSTs for applications that aim at a robust isolation of the local effects.

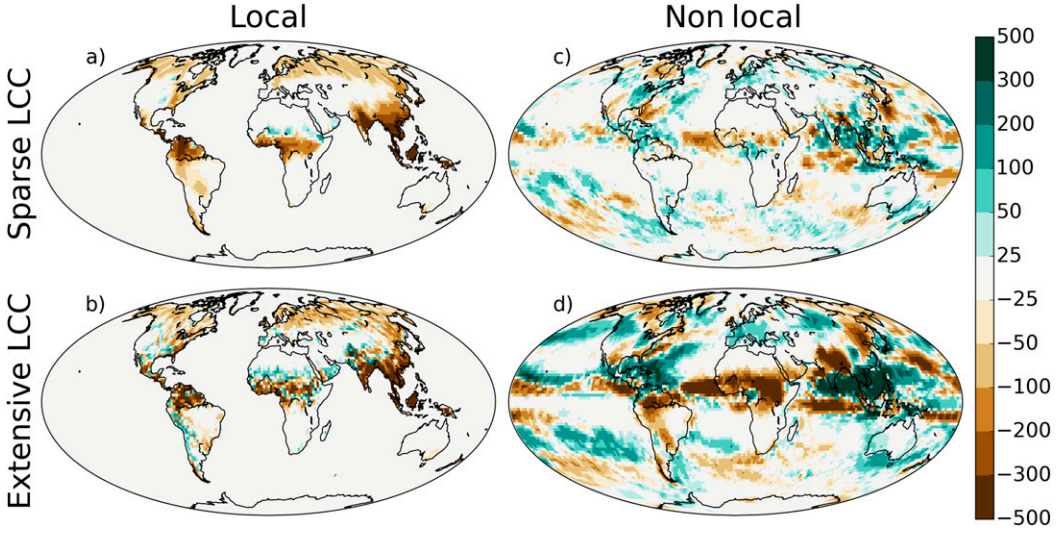

FIG. B4. As in Fig. B3, but for boreal summer (JJA). Note the nonlinear scale.

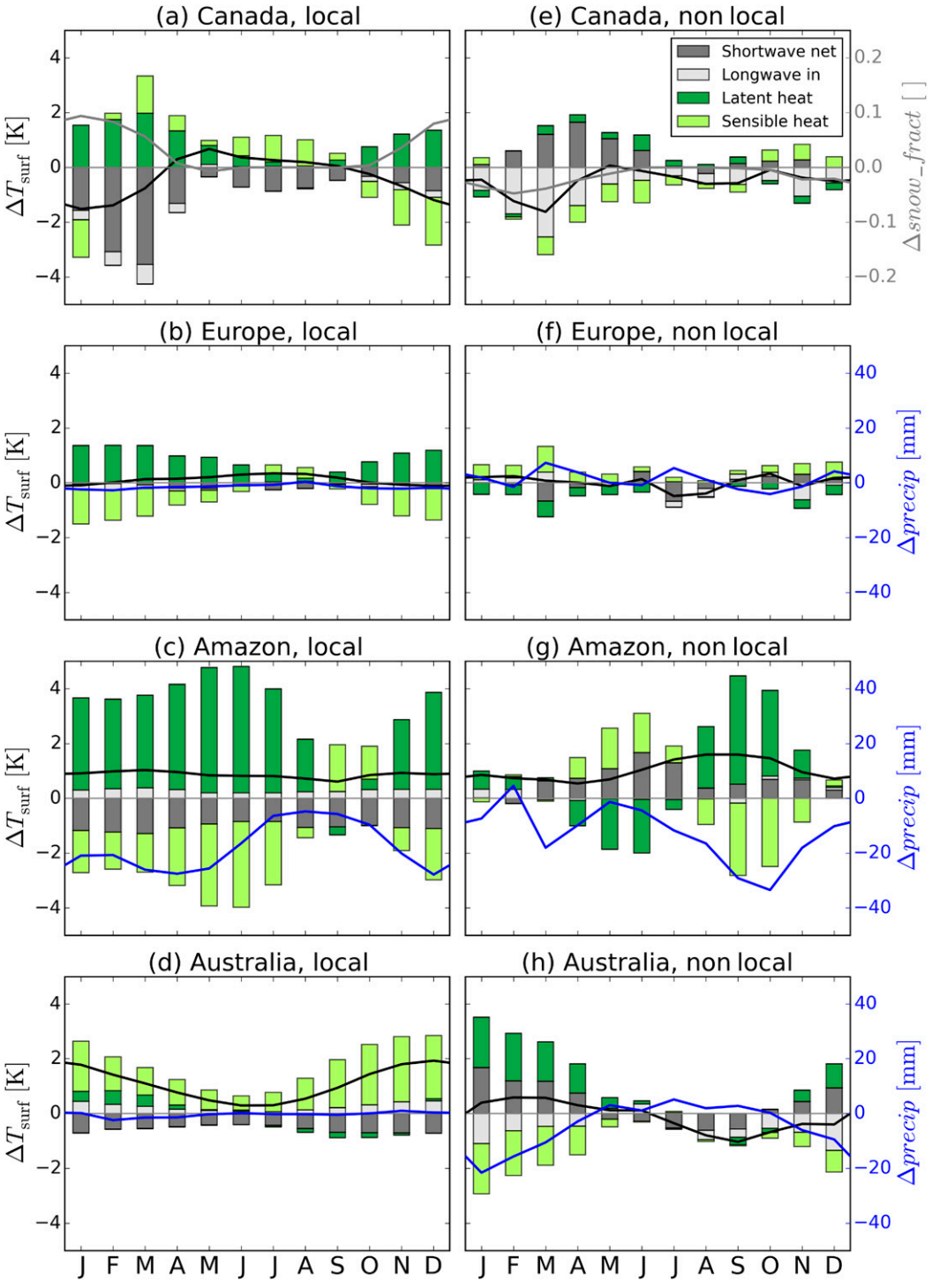

FIG. B5. Energy balance decomposition of monthly mean changes in surface temperature T_{surf} (K) caused by extensive deforestation. Shown are (a)–(d) local effects and (e)–(h) nonlocal effects as averages over regions indicated in Fig. C1b. The bars represent surface temperature changes due to changes in components of the surface energy budget. The black line indicates total changes in surface temperature, which is approximately the sum of the bars in the respective month. The blue and gray lines indicate changes in precipitation (precip) and snow cover fraction (snow_fract), respectively.

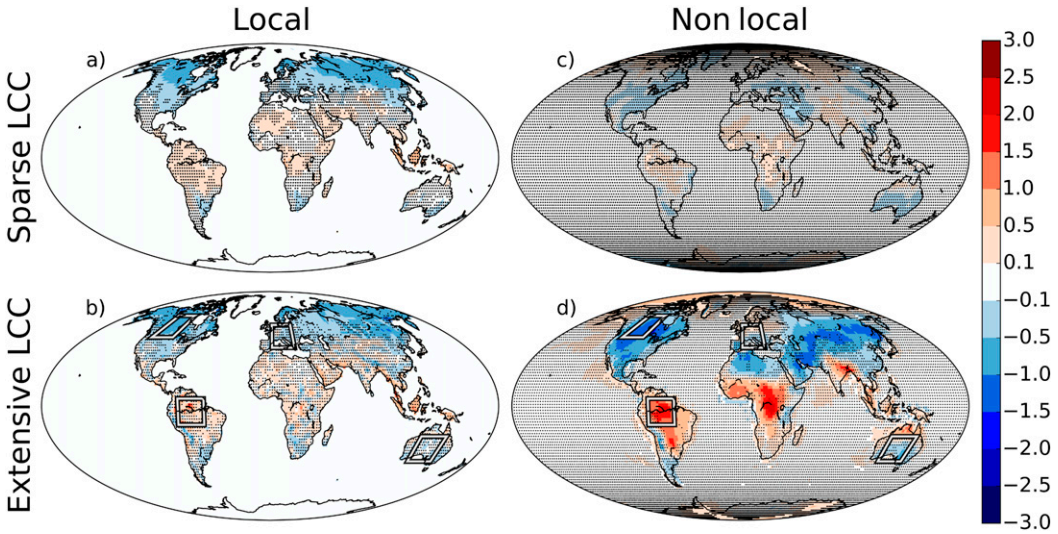

FIG. C1. Difference in mean 2-m air temperature (K) for (a),(c) sparse and (b),(d) extensive deforestation. (a),(b) Local effects and (c),(d) nonlocal effects. Statistical significance is calculated according to a 5% level in Student's *t* test accounting for autocorrelation (Zwiers and von Storch 1995). Note that we mark grid boxes that are not statistically significant. The regions shown as rectangles in (b),(d) denote areas selected for the regional energy balance decomposition in Fig. B5.

We acknowledge that land surface models differ in their methods of implementing LCC (Pitman et al. 2009). Thus, the results presented here, both for local and nonlocal effects, are specific for our model (MPI-ESM), in particular for exact quantifications. However, the approach presented in this study opens ways to an intercomparison of local and nonlocal effects across climate models. If models disagree mainly with respect to the nonlocal effects, this would hint at large-scale advective processes and changes in global circulation to be responsible for intermodel differences. However, an intermodel spread in the local effects would suggest a different representation of processes relevant within a grid box to be responsible for the intermodel uncertainties. Thus, because of their different nature, analyzing local and nonlocal effects separately allows for a deeper process understanding of LCC effects in climate models.

An isolation of the local effects has a wide range of applications in the LCC context. As we illustrated, isolation of the local effects enables a consistent comparison to observed climate effects of LCC, such as ground-based (e.g., Lee et al. 2011; Zhang et al. 2014) or remote sensing studies (e.g., Li et al. 2015; Alkama and Cescatti 2016). Further studies can investigate whether nighttime and daytime effects of LCC (e.g., Lee et al. 2011; Li et al. 2015) are well represented in climate models and whether models correctly capture the effects on temperature and precipitation during extreme events, as in the study by Teuling et al. (2010). As weather-related noise and advection processes are largely excluded from the local effects, they can be employed to determine the influence of land–atmosphere coupling strength on the LCC effects, as performed for the total biogeophysical effects by Lorenz and Pitman (2014).

In a broader context, the method described here of separating local and nonlocal effects is not restricted to LCC studies but can be employed in studies focusing on any land surface process that is mainly acting locally but capable of influencing wide-ranging climate when applied on a larger scale. For instance, this method could be used in studies on the climate effects of irrigation or wildfires. Analogous to the findings in our study, isolating local effects can improve signal-to-noise ratio in realistic scenarios. Additionally, the method of separating local and nonlocal effects can be used in idealized large-scale studies and enhance understanding of processes influencing local and large-scale climate.

Acknowledgments. We thank Gitta Lasslop, Nathalie de Noblet-Ducoudré, and two anonymous reviewers for helpful comments, which greatly helped to improve the manuscript, and Julia Nabel and Thomas Raddatz for technical support. We thank Yan Li for providing access to the satellite observation data (see Li 2016). The simulations were performed at the German Climate Computing Centre (DKRZ). This work was supported by the German Research Foundation's Emmy Noether Program. Primary data and scripts used in the analysis and other supplementary information that may be useful in reproducing the authors' work are archived by the

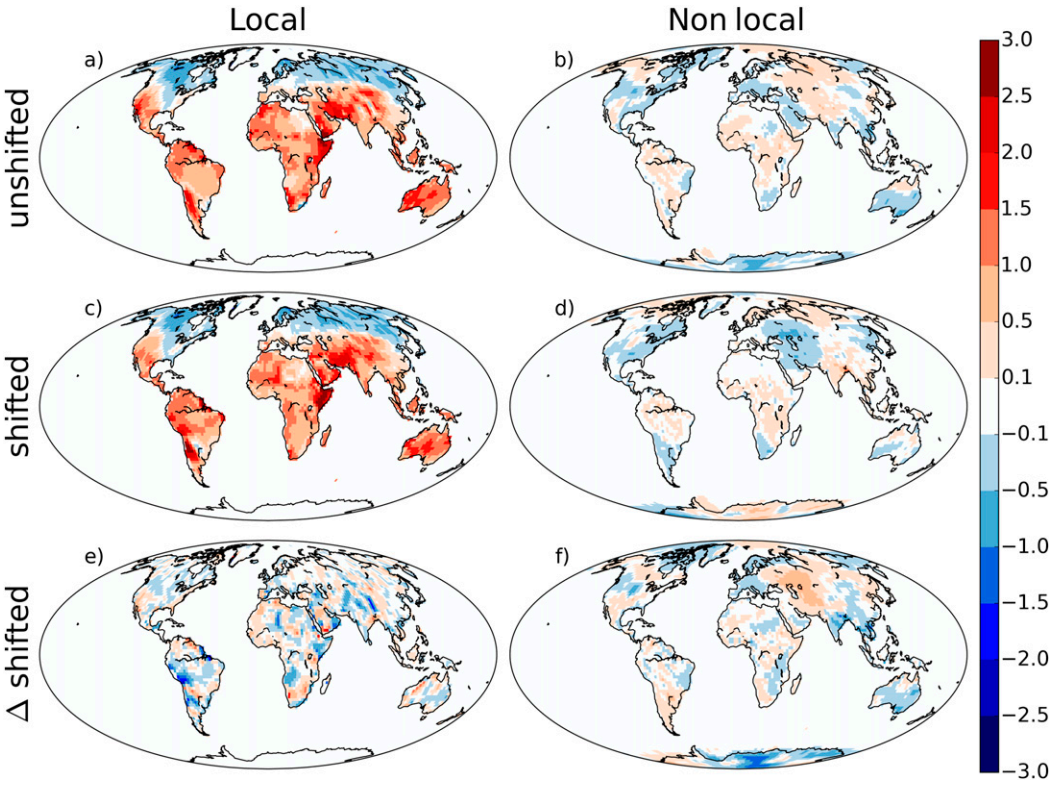

FIG. D1. Analysis of interpolation error for changes in surface temperature (K) due to sparse LCC. Shown are the (a),(c),(e) local effects and (b),(d),(f) nonlocal effects of (a),(b) the unshifted simulations, (c),(d) the shifted simulations, and (e),(f) the differences between unshifted and shifted simulations.

Max Planck Institute for Meteorology and can be obtained by contacting publications@mpimet.mpg.de.

APPENDIX A

Number of Necessary Simulation Years for a Robust Estimation of the Local Effects

Throughout this paper we use 30 years of simulations in our data analysis. To assess whether those 30 years are sufficient to identify the local contribution, we create an ensemble of five members for sparse LCC. For each of those members, we compare the mean of the first k years against the mean of all the years of the remaining four members for the local effects and the simulated signal, respectively. As a measure of inaccuracy, we calculate the root-mean-square (RMS) deviation between the two maps, evaluated at all LCC boxes. Figure A1 illustrates that, for sparse LCC, the RMS deviation is lower for the local effects than for the simulated signal. For the local effects, the RMS deviation seems to stabilize after 30 years, indicating that simulating longer than 30 years does not markedly increase the accuracy of the results.

APPENDIX B

Regional Analysis of Seasonality for Extensive LCC

Here we provide additional evidence for local and nonlocal effects being qualitatively different. For this purpose, we explore the seasonality of local and nonlocal effects separately. Local and nonlocal effects for boreal winter (DJF) and summer (JJA) are shown in Figs. B1–B4 for changes in surface temperature and precipitation. The local changes in surface temperature vary seasonally; in the high northern latitudes, the local effects in winter are a cooling of up to 3 K (Fig. B1b), while in summer the local effects are a warming of up to 0.5 K (Fig. B2b). In contrast, the nonlocal effects on surface temperature have the same sign in DJF and JJA in large parts of the boreal zone, such as northern Asia and Canada (Fig. B1d vs Fig. B2d). For precipitation, the largest difference between DJF and JJA is the location of zones in the tropics/subtropics where LCC leads to a reduction in precipitation; these zones are farther north in JJA for both local and nonlocal effects (Figs. B3 and B4).

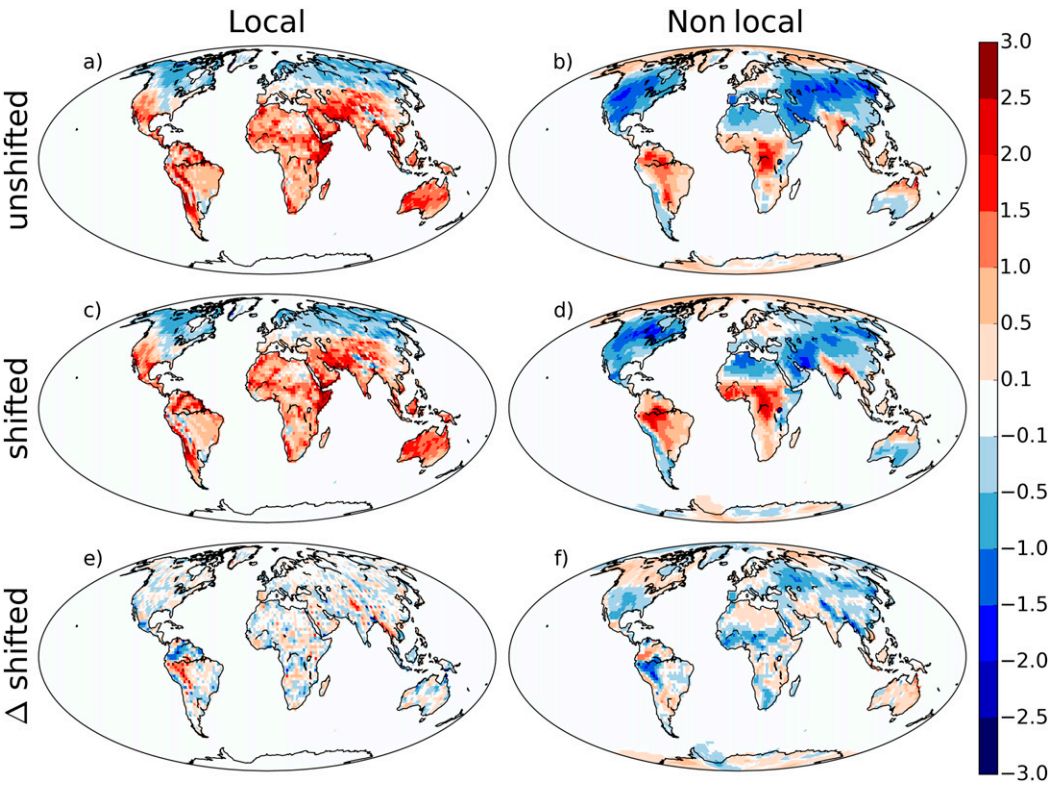

FIG. D2. As in Fig. D1, but for extensive LCC.

While the maps presented in Figs. B1–B4 provide information about the seasonality of LCC-induced changes in surface temperature and precipitation, these figures do not give insight into the underlying mechanisms. We select four regions (indicated by rectangles in Fig. C1) where we identify the dominant mechanisms for local and nonlocal effects of extensive LCC in different climate regimes. To this end, we perform an energy balance decomposition in these four regions and present the results in Fig. B5.

Canada and Europe represent temperate regions with and without long-lasting snow cover. The local cooling in Canada in the winter and spring months (which is not apparent in Europe) originates from a reduction in shortwave net radiation, induced by an increase in surface albedo due to a combination of the local increase in snow cover and the loss of snow masking after deforestation. In contrast, the nonlocal effects exhibit an increase in shortwave net radiation, which partly originates from a nonlocal decrease in snow cover. The Amazon and Australia represent regions with humid and arid tropical/subtropical conditions, respectively. The local changes in latent and sensible heat in the Amazon are presumably linked to the LCC-induced changes in local evapotranspirative efficiency but also to local changes in precipitation. The local changes in sensible heat in Australia presumably originate from the local LCC-induced decrease in surface roughness. In contrast, the nonlocal changes in latent and sensible heat in Australia seem to be driven by the changes in precipitation. Local and nonlocal effects can differ in sign (e.g., local increase vs nonlocal decrease in snow cover fraction in Canada) and seasonality of the respective climatic drivers (e.g., precipitation in the Amazon).

APPENDIX C

Results for 2-m Air Temperature

Fig. C1 shows results analogous to Fig. 2 for 2-m air temperature for comparison against other published or follow-up studies. The conclusions are qualitatively the same as for surface temperature and precipitation: the two local effects are similar, while the nonlocal effects differ substantially. Note that the local effects on 2-m air temperature in our model are substantially weaker than the effects on surface temperature. In contrast to the local effects, our nonlocal effects influence 2-m air temperature and surface temperature to a similar degree (Fig. 2d vs Fig. C1d).

This different impact of local and nonlocal effects on 2-m air temperature may arise from the different

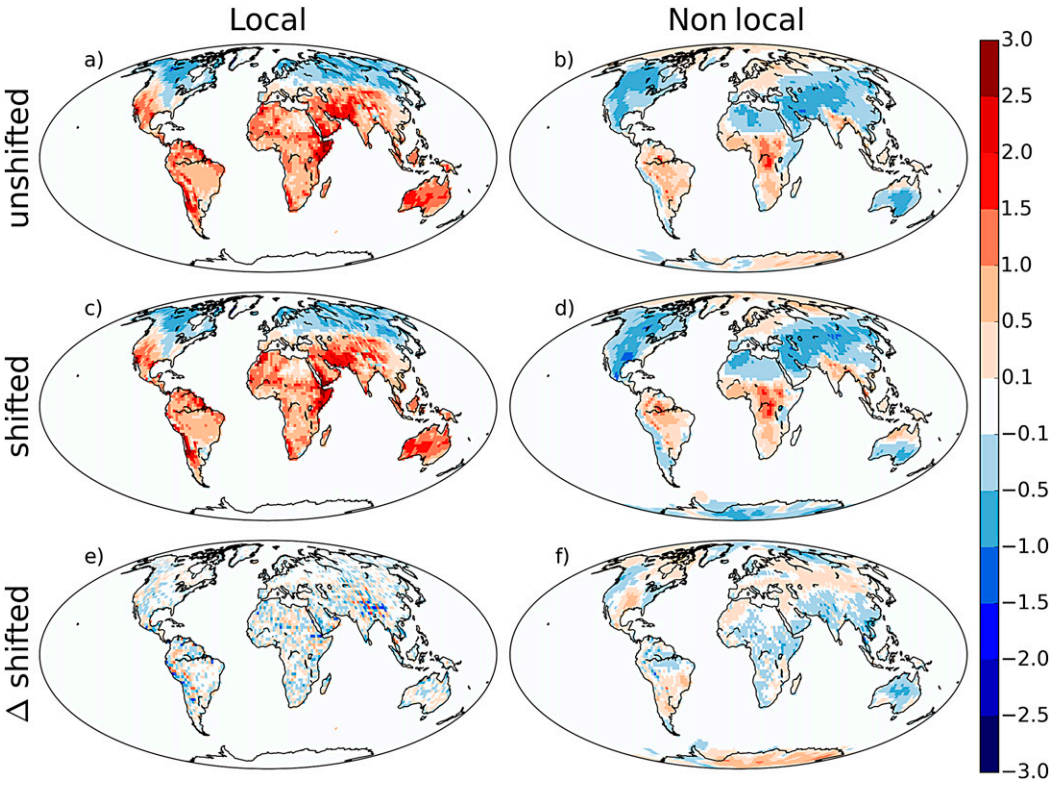

FIG. D3. As in Fig. D1, but for chessboard LCC.

underlying mechanisms; the local effects originate from changes in local surface properties and the land surface directly responds, while the lowest atmospheric layer (which represents the lowest ~40 m) mainly adjusts to these changes in surface variables. This adjustment is incomplete, as some of the signal is diluted by horizontal advection. In MPI-ESM, 2-m air temperature is calculated by interpolation between surface temperature and the lowest level of the atmosphere, based on Monin–Obukhov similarity theory. Thus, similar to the

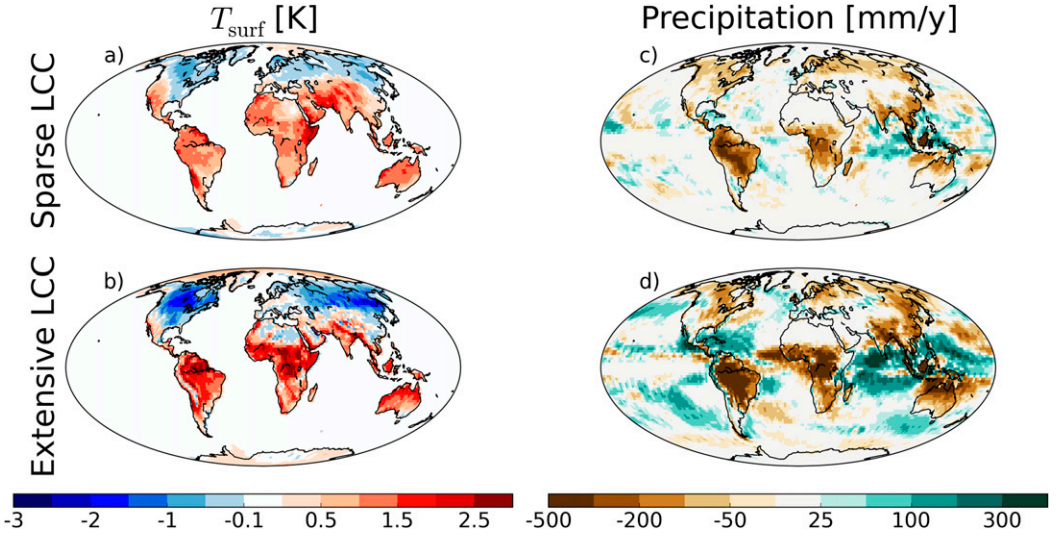

FIG. E1. Sums of local and nonlocal effects for (a),(c) sparse and (b),(d) extensive deforestation. (a),(b) Changes in surface temperature (K) and (c),(d) changes in precipitation (mm yr^{-1}). Note the nonlinear scale.

lowest atmospheric layer, 2-m air temperature is less affected by LCC compared to surface temperature. In contrast, the nonlocal effects (e.g., changes in global circulation patterns) primarily affect the atmosphere, and the land surface variables adjust to the changed atmospheric conditions. Because the signal in the land grid boxes is not diluted by advection to adjacent land grid boxes, the surface temperature can fully adjust to the changed atmospheric conditions. Thus, the nonlocal effects on surface temperature and 2-m air temperature are almost equally affected by LCC.

APPENDIX D

Interpolation Method and Interpolation Errors

The separation method includes horizontal interpolation between grid cells for the isolation of both local and nonlocal effects. Inland, where data points with known values are available at all four surrounding sides, we apply bilinear interpolation. At coastal regions, where values for at least one side are missing, we apply nearest-neighbor extrapolation. For simplification, we refer to this combination of interpolation and extrapolation as ''interpolation'' here and in the main text.

To assess errors associated with this interpolation, the simulations with the LCC boxes at their original location (''unshifted'') are complemented with additional simulations. In these additional simulations, we shift the LCC boxes by two (''shifted''). We isolate local and nonlocal effects separately for the unshifted and shifted simulations, both for sparse LCC (Fig. D1) and for extensive LCC (Fig. D2). Considering the nonlocal effects, a fair amount of interannual variability can be seen in the differences between the unshifted and shifted versions (see Fig. D1f). The local effects are by construction largely free of this interannual variability, so the differences between unshifted and shifted local effects largely consist of interpolation errors. Furthermore, the local effects already include the interpolation errors from the nonlocal effects (via the step in Fig. 1d of the step-by-step instruction of the separation approach in the main text). Thus, when analyzing the overall interpolation errors, we focus on the local effects in the following.

The shifted and unshifted local effects are generally in good agreement (Fig. D1a vs Fig. D1c; Fig. D2a vs Fig. D2c). Globally, the interpolation errors are similar for sparse and extensive LCC: the root-mean-square difference over land between the unshifted and shifted local effects is 0.35 K for sparse LCC and 0.39 K for extensive LCC. In some regions, the interpolation errors cannot be neglected, especially in the surroundings of mountain ranges such as the Andes or the Himalayas (Figs. D1e and D2e) where the interpolation errors are larger than 1 K. Thus, for the analysis in the main text, we consider the combined information from shifted and unshifted simulations in order to decrease the dependence on the exact location of the LCC boxes.

In follow-up studies that require an isolation of the local effects, the horizontal interpolation errors can be reduced as follows: Instead of choosing a sparse or extensive pattern in the isolation approach, a chessboard-like pattern of altering one out of two grid boxes may be chosen. Thus, the calculation of both local and nonlocal effects requires horizontal interpolation only from directly adjacent grid boxes. This ''chessboard LCC'' reduces the horizontal interpolation errors (see Fig. D3e); the root-mean-square difference over land between the unshifted and shifted local effects is then reduced to 0.29 K.

APPENDIX E

Total Local plus Nonlocal Effects

To give an idea about the total (local plus nonlocal) effects of extensive deforestation, we provide the sum of local and nonlocal effects for changes in surface temperature and precipitation (Fig. E1). The surface temperature change maps were obtained by adding the local and nonlocal effects of Fig. 2. The precipitation change maps were obtained by adding the local and nonlocal effects of Fig. 3. Because the nonlocal effects of sparse LCC are small, the local plus nonlocal effects of sparse deforestation are similar to the local effects alone. In contrast, the strong nonlocal effects of extensive LCC magnify the local effects in some regions, as can be seen in the inner tropics or the high northern latitudes.

REFERENCES

Alkama, R., and A. Cescatti, 2016: Biophysical climate impacts of recent changes in global forest cover. *Science*, **351**, 600–604, doi:10.1126/science.aac8083.

Bala, G., K. Caldeira, M. Wickett, T. J. Phillips, D. B. Lobell, C. Delire, and A. Mirin, 2007: Combined climate and carbon-cycle effects of large-scale deforestation. *Proc. Natl. Acad. Sci. USA*, **104**, 6550–6555, doi:10.1073/pnas.0608998104.

Bathiany, S., M. Claussen, V. Brovkin, T. Raddatz, and V. Gayler, 2010: Combined biogeophysical and biogeochemical effects of large-scale forest cover changes in the MPI Earth system model. *Biogeosciences*, **7**, 1383–1399, doi:10.5194/bg-7-1383-2010.

Boisier, J. P., and Coauthors, 2012: Attributing the impacts of land-cover changes in temperate regions on surface temperature and heat fluxes to specific causes: Results from the first LUCID set of simulations. *J. Geophys. Res.*, **117**, D12116, doi:10.1029/2011JD017106.

Bonan, G. B., 2008: Forests and climate change: Forcings, feedbacks, and the climate benefits of forests. *Science*, **320**, 1444–1449, doi:10.1126/science.1155121.

Boysen, L. R., V. Brovkin, V. K. Arora, P. Cadule, N. de Noblet-Ducoudré, E. Kato, J. Pongratz, and V. Gayler, 2014: Global and regional effects of land-use change on climate in 21st century simulations with interactive carbon cycle. *Earth Syst. Dynam.*, **5**, 309–319, doi:10.5194/esd-5-309-2014.

Brovkin, V., L. Boysen, T. Raddatz, V. Gayler, A. Loew, and M. Claussen, 2013: Evaluation of vegetation cover and land-surface albedo in MPI-ESM CMIP5 simulations. *J. Adv. Model. Earth Syst.*, **5**, 48–57, doi:10.1029/2012MS000169.

Claussen, M., V. Brovkin, and A. Ganopolski, 2001: Biogeophysical versus biogeochemical feedbacks of large-scale land cover change. *Geophys. Res. Lett.*, **28**, 1011–1014, doi:10.1029/2000GL012471.

Davin, E. L., and N. de Noblet-Ducoudré, 2010: Climatic impact of global-scale deforestation: Radiative versus nonradiative processes. *J. Climate*, **23**, 97–112, doi:10.1175/2009JCLI3102.1.

de Noblet-Ducoudré, N., and Coauthors, 2012: Determining robust impacts of land-use-induced land cover changes on surface climate over North America and Eurasia: Results from the first set of LUCID experiments. *J. Climate*, **25**, 3261–3281, doi:10.1175/JCLI-D-11-00338.1.

Deser, C., R. Knutti, S. Solomon, and A. S. Phillips, 2012: Communication of the role of natural variability in future North American climate. *Nat. Climate Change*, **2**, 775–779, doi:10.1038/nclimate1562.

Devaraju, N., G. Bala, and A. Modak, 2015: Effects of large-scale deforestation on precipitation in the monsoon regions: Remote versus local effects. *Proc. Natl. Acad. Sci. USA*, **112**, 3257–3262, doi:10.1073/pnas.1423439112.

Gibbard, S., K. Caldeira, G. Bala, T. J. Phillips, and M. Wickett, 2005: Climate effects of global land cover change. *Geophys. Res. Lett.*, **32**, L23705, doi:10.1029/2005GL024550.

Giorgetta, M. A., and Coauthors, 2013: The atmospheric general circulation model ECHAM6—Model description. Max Planck Institute for Meteorology Tech. Rep. 135, 173 pp.

Goessling, H. F., and C. H. Reick, 2011: What do moisture recycling estimates tell us? Exploring the extreme case of non-evaporating continents. *Hydrol. Earth Syst. Sci.*, **15**, 3217–3235, doi:10.5194/hess-15-3217-2011.

Hagemann, S., A. Loew, and A. Andersson, 2013: Combined evaluation of MPI-ESM land surface water and energy fluxes. *J. Adv. Model. Earth Syst.*, **5**, 259–286, doi:10.1029/2012MS000173.

Hurtt, G. C., and Coauthors, 2011: Harmonization of land-use scenarios for the period 1500–2100: 600 years of global gridded annual land-use transitions, wood harvest, and resulting secondary lands. *Climatic Change*, **109**, 117–161, doi:10.1007/s10584-011-0153-2.

IPCC, 2013: *Climate Change 2013: The Physical Science Basis*. Cambridge University Press, 1535 pp., doi:10.1017/CBO9781107415324.

Kumar, S., P. A. Dirmeyer, V. Merwade, T. DelSole, J. M. Adams, and D. Niyogi, 2013: Land use/cover change impacts in CMIP5 climate simulations: A new methodology and 21st century challenges. *J. Geophys. Res. Atmos.*, **118**, 6337–6353, doi:10.1002/jgrd.50463.

Lee, X., and Coauthors, 2011: Observed increase in local cooling effect of deforestation at higher latitudes. *Nature*, **479**, 384–387, doi:10.1038/nature10588.

Lejeune, Q., E. L. Davin, B. P. Guillod, and S. I. Seneviratne, 2015: Influence of Amazonian deforestation on the future evolution of regional surface fluxes, circulation, surface temperature and precipitation. *Climate Dyn.*, **44**, 2769–2786, doi:10.1007/s00382-014-2203-8.

Li, Y., 2016: Dataset for paper ''Local cooling and warming effects of forest based on satellite data.'' Figshare, accessed 21 September 2016, doi:10.6084/m9.figshare.2445310.v1.

——, M. Zhao, S. Motesharrei, Q. Mu, E. Kalnay, and S. Li, 2015: Local cooling and warming effects of forests based on satellite observations. *Nat. Commun.*, **6**, 6603, doi:10.1038/ncomms7603.

Lorenz, R., and A. J. Pitman, 2014: Effect of land-atmosphere coupling strength on impacts from Amazonian deforestation. *Geophys. Res. Lett.*, **41**, 5987–5995, doi:10.1002/2014GL061017.

Luyssaert, S., and Coauthors, 2014: Land management and land-cover change have impacts of similar magnitude on surface temperature. *Nat. Climate Change*, **4**, 389–393, doi:10.1038/nclimate2196.

Mahlstein, I., R. Knutti, S. Solomon, and R. W. Portmann, 2011: Early onset of significant local warming in low latitude countries. *Environ. Res. Lett.*, **6**, 034009, doi:10.1088/1748-9326/6/3/034009.

Malyshev, S., E. Shevliakova, R. J. Stouffer, and S. W. Pacala, 2015: Contrasting local versus regional effects of land-use-change-induced heterogeneity on historical climate: Analysis with the GFDL Earth system model. *J. Climate*, **28**, 5448–5469, doi:10.1175/JCLI-D-14-00586.1.

Pitman, A. J., and Coauthors, 2009: Uncertainties in climate responses to past land cover change: First results from the LUCID intercomparison study. *Geophys. Res. Lett.*, **36**, L14814, doi:10.1029/2009GL039076.

——, F. B. Avila, G. Abramowitz, Y. P. Wang, S. J. Phipps, and N. de Noblet-Ducoudré, 2011: Importance of background climate in determining impact of land-cover change on regional climate. *Nat. Climate Change*, **1**, 472–475, doi:10.1038/nclimate1294.

Pongratz, J., C. Reick, T. Raddatz, and M. Claussen, 2008: A reconstruction of global agricultural areas and land cover for the last millennium. *Global Biogeochem. Cycles*, **22**, GB3018, doi:10.1029/2007GB003153.

Reick, C. H., T. Raddatz, V. Brovkin, and V. Gayler, 2013: Representation of natural and anthropogenic land cover change in MPI-ESM. *J. Adv. Model. Earth Syst.*, **5**, 459–482, doi:10.1002/jame.20022.

Rotenberg, E., and D. Yakir, 2010: Contribution of semi-arid forests to the climate system. *Science*, **327**, 451–454, doi:10.1126/science.1179998.

Swann, A. L. S., I. Y. Fung, and J. C. H. Chiang, 2012: Mid-latitude afforestation shifts general circulation and tropical precipitation. *Proc. Natl. Acad. Sci. USA*, **109**, 712–716, doi:10.1073/pnas.1116706108.

Teuling, A. J., and Coauthors, 2010: Contrasting response of European forest and grassland energy exchange to heatwaves. *Nat. Geosci.*, **3**, 722–727, doi:10.1038/ngeo950.

West, P. C., G. T. Narisma, C. C. Barford, C. J. Kucharik, and J. A. Foley, 2011: An alternative approach for quantifying climate regulation by ecosystems. *Front. Ecol. Environ.*, **9**, 126–133, doi:10.1890/090015.

Zhang, W., C. Jansson, P. A. Miller, B. Smith, and P. Samuelsson, 2014: Biogeophysical feedbacks enhance the Arctic terrestrial carbon sink in regional Earth system dynamics. *Biogeosciences*, **8**, 5503–5519, doi:10.5194/bg-11-5503-2014.

Zwiers, F. W., and H. von Storch, 1995: Taking serial correlation into account in tests of the mean. *J. Climate*, **8**, 336–351, doi:10.1175/1520-0442(1995)008<0336:TSCIAI>2.0.CO;2.